Electronic Supplementary Material (ESI) for New Journal of Chemistry.

High-performance photocatalyst for overall water splitting: type-II $WSi_2N_4/MoSi_2N_4$ heterostructure

*Jiading Bao,[a] Ye Wang,[a] Xiaodong Liu,[a] Rui Zhao,[b] * Jiabing Yu,[c] Xianping Chen [c]*

[a] Guangxi Key Laboratory of Manufacturing Systems and Advanced Manufacturing Technology, Faculty of Mechanical and Electrical Engineering, Guilin University of Electronic Technology, Guilin, 541004, China.

[b] School of Language and Literature, Guilin University, Guilin, 541006, China.

[c] Key Laboratory of Optoelectronic Technology & Systems, Education Ministry of China, Chongqing University and College of Optoelectronic Engineering, Chongqing University, Chongqing, 400044, China.

Table S1. The lattice coefficients (Å) of single layers within the MA_2Z_4 family; the cohesive energy per atom (E_{coh}); Bandgap E_g^{PBE} and E_g^{HSE} are calculated using PBE and HSE06, respectively.

	Lattice constant (Å)	E_{coh} (eV)/atom	E_g^{PBE} (eV)	E_g^{HSE} (eV)
$MoSi_2P_4$	3.469	-6.596	0.685	0.971
$MoSi_2As_4$	3.626	-5.865	0.594	0.840
$CrSi_2N_4$	2.845	-8.022	0.495	0.966
VSi_2N_4	2.875	-8.132	---	---
$NbSi_2N_4$	2.925	-8.112	---	---
$TaSi_2N_4$	2.975	-8.542	---	---

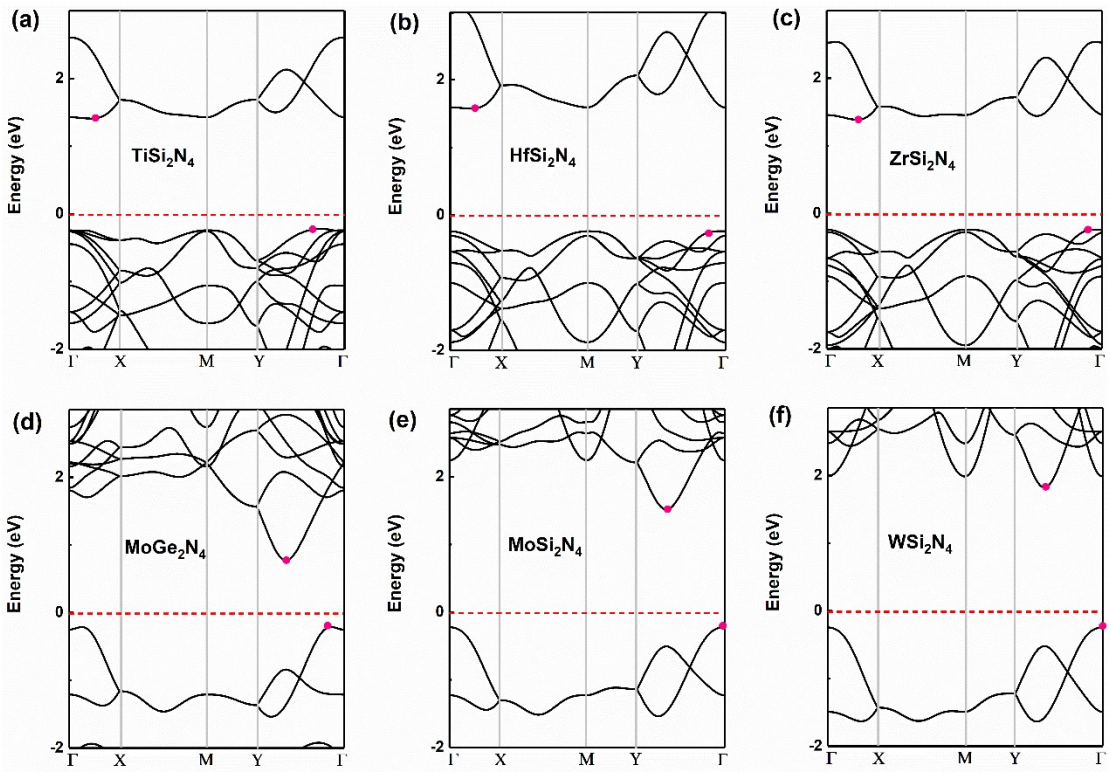

Fig. S1 Band structures of single-layer MA_2Z_4 family calculated with the HSE06 method. The conduction band minimum (CBM) and valence band maximum (VBM) are shown with red solid origin marks. The Fermi-level is at zero energy. All six monolayers are indirect bandgap semiconductors.

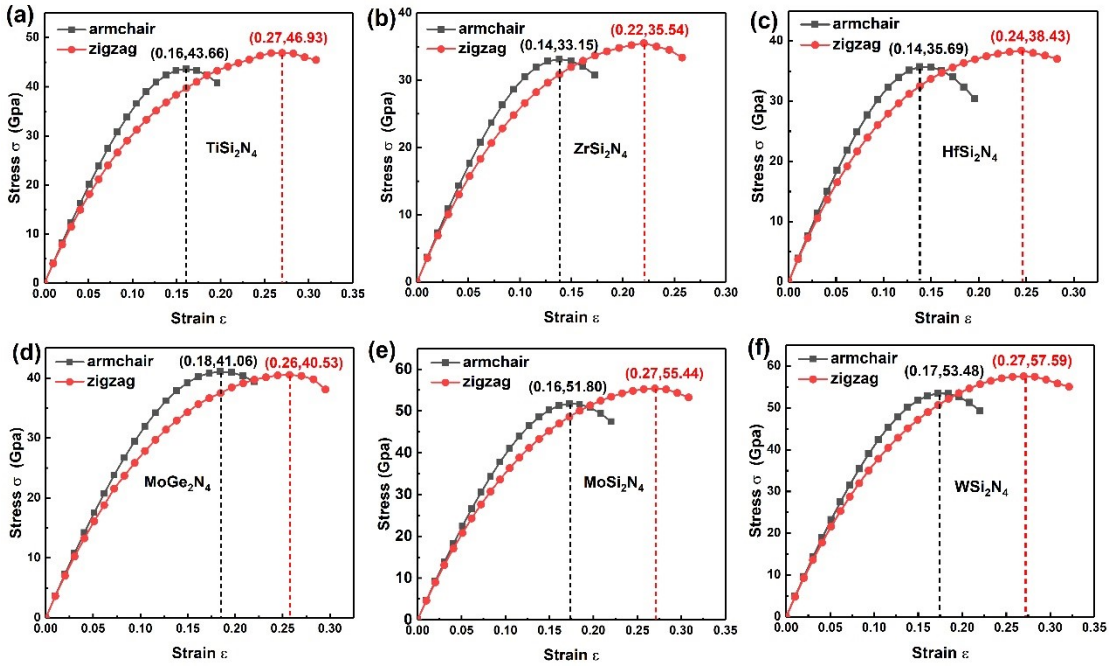

Fig. S2 Stress-strain curves calculated by DFT of single-layer MA_2N_4 family along the zigzag and armchair directions. The red and black curves are along the zigzag and armchair directions, respectively. In the beginning, the trend of the stress-strain curve along both the zigzag and armchair directions shows non-linear increase. In response to increasing strain and the stress intensity reaching the maximum value, there follows a decrease in the stress-strain curve, indicating the broken atomic bond.

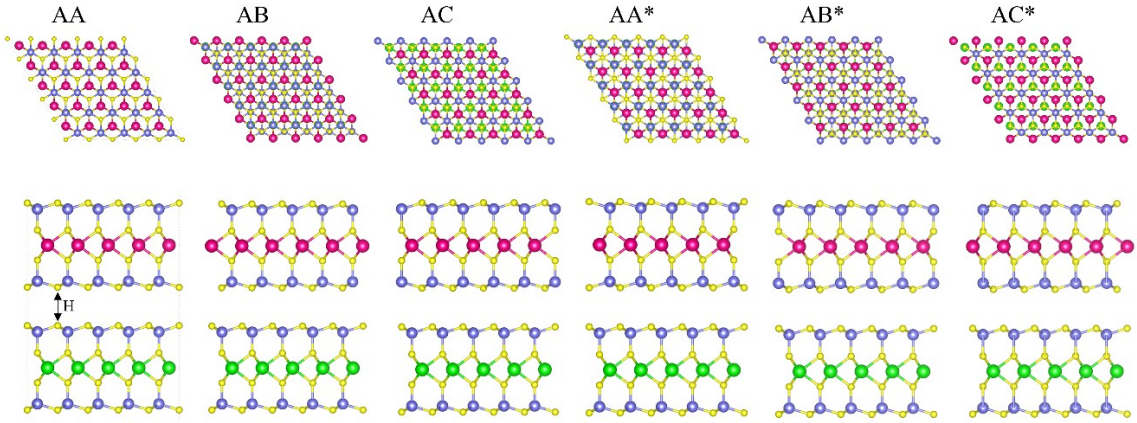

Fig. S3 The schematic illustration showcases six different stacking configurations of $WSi_2N_4/MoSi_2N_4$ heterostructures.

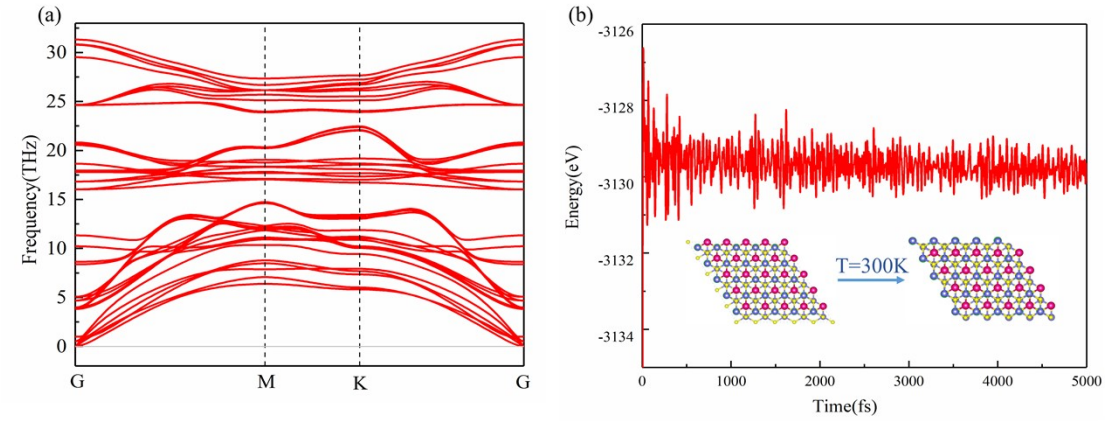

Fig. S4 (a) Phonon dispersion spectrum of $WSi_2N_4/MoSi_2N_4$ heterostructure. (b) AIMD simulations of the $WSi_2N_4/MoSi_2N_4$ heterostructure at the temperature of 300 K during 5ps.

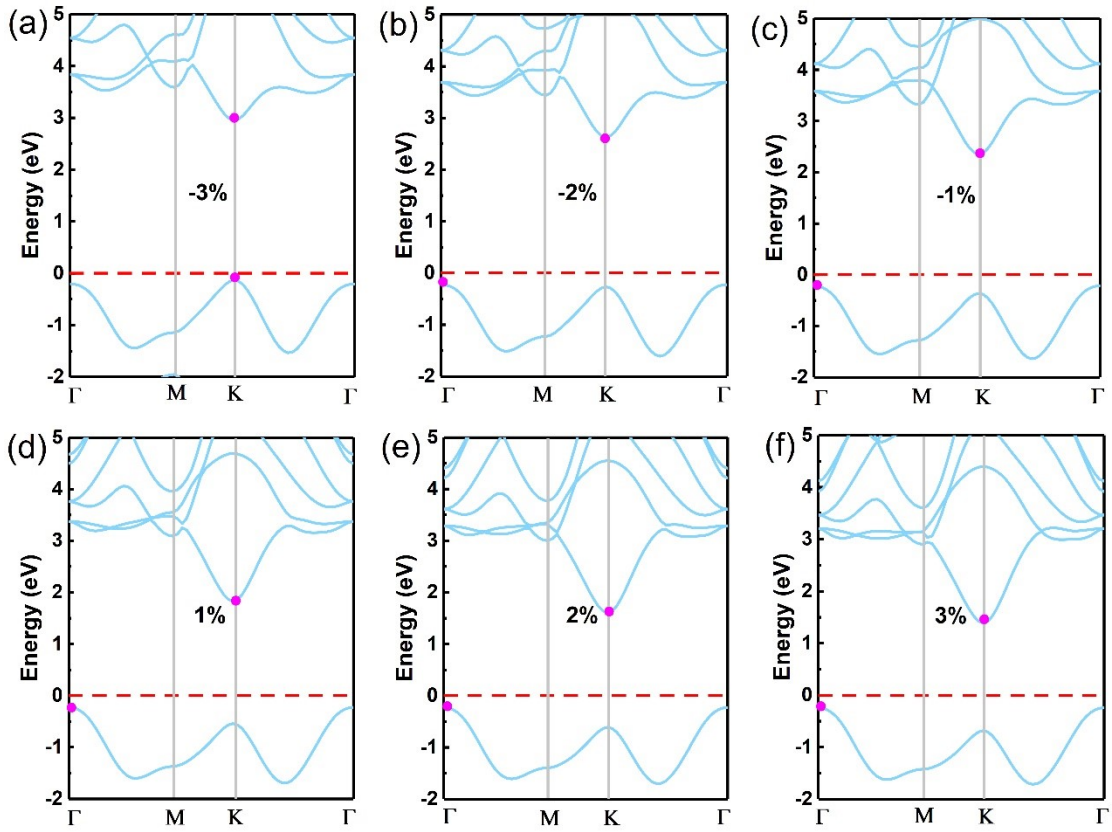

Fig. S5 Energy band structure of different biaxial strain conditions. The pink dots are the conduction band minimum (CBM) and valence band maximum (VBM), respectively. The $WSi_2N_4/MoSi_2N_4$ heterostructure is a direct bandgap semiconductor at -3% biaxial strain. As the strain changes, it transforms into indirect bandgap semiconductor.

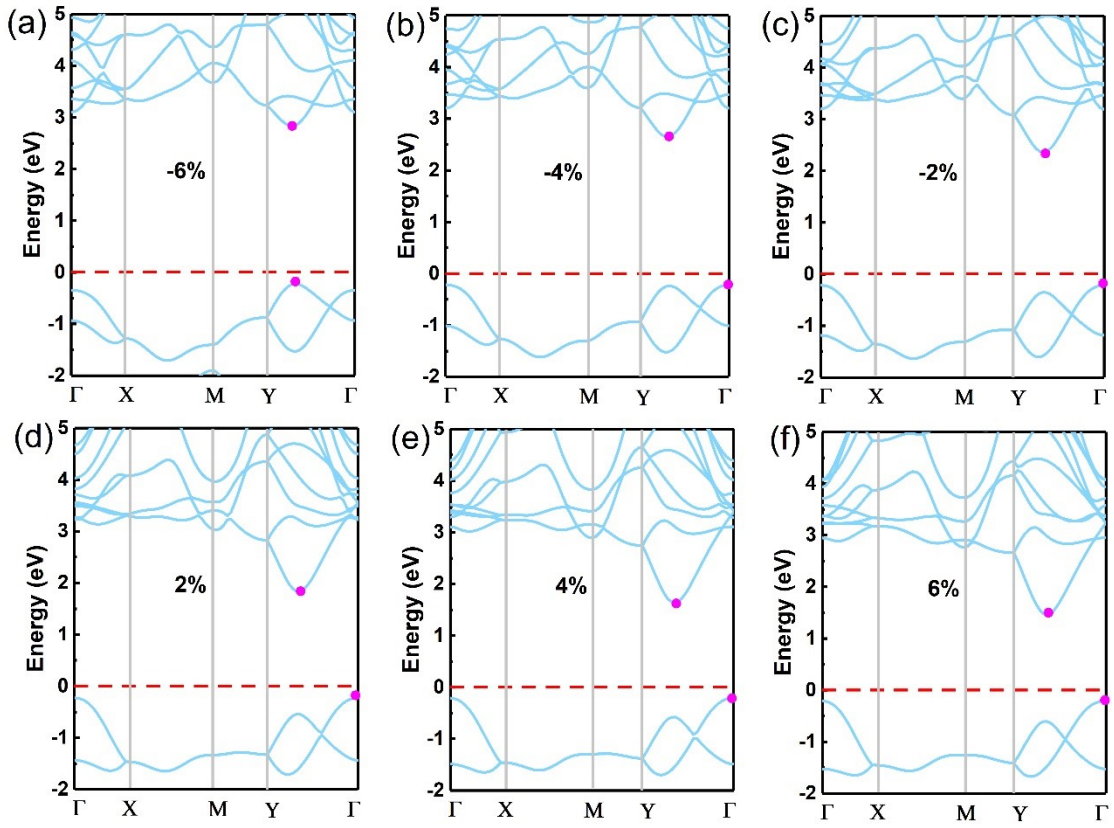

Fig. S6 Energy band structure of different uniaxial strain conditions in the x-direction. The pink dots are the conduction band minimum (CBM) and valence band maximum (VBM), respectively. The $WSi_2N_4/MoSi_2N_4$ heterostructure is a direct bandgap semiconductor at -6% uniaxial strain. As the strain changes, it transforms into indirect bandgap semiconductor.

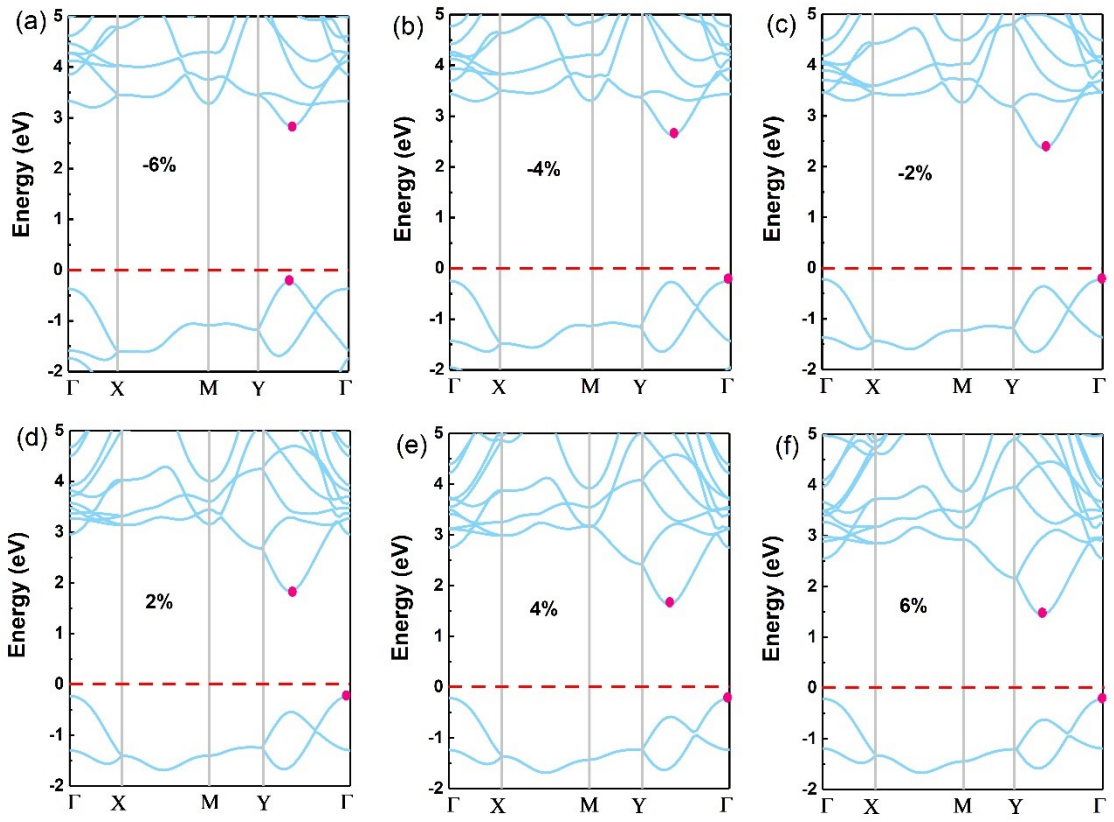

Fig. S7 Energy band structure of different uniaxial strain conditions in the y-direction. The pink dots are the conduction band minimum (CBM) and valence band maximum (VBM), respectively. The $WSi_2N_4/MoSi_2N_4$ heterostructure is a direct bandgap semiconductor at -6% uniaxial strain. As the strain changes, it transforms into indirect bandgap semiconductor.